IN-PAVEMENT FIBER BRAGG GRATING SENSORS FOR WEIGHT-IN-MOTION

MEASUREMENTS


A Thesis
Submitted to the Graduate Faculty
of the
North Dakota State University
of Agriculture and Applied Science


By

Mu'ath Ahmad Al-Tarawneh


In Partial Fulfillment of the Requirements
for the Degree of
MASTER OF SCIENCE


Major Department:
Civil and Environmental Engineering


March 2016


Fargo, North Dakota

# North Dakota State University
## Graduate School

**Title**

IN-PAVEMENT FIBER BRAGG GRATING SENSORS FOR WEIGHT-
IN-MOTION MEASUREMENTS

**By**

Mu'ath Ahmad Al-Tarawneh

The Supervisory Committee certifies that this *disquisition* complies with North Dakota

State University's regulations and meets the accepted standards for the degree of

**MASTER OF SCIENCE**

SUPERVISORY COMMITTEE:

Dr.Ying Huang

Chair

Dr. Magdy Abdelrahman

Dr. Zhili" Jerry" Gao

Approved:

| 03/31/2016 | Dr. Dinesh Katti |
|---|---|
| Date | Department Chair |

**ABSTRACT**

Estimation a traffic over the design period is one of the critical factors in pavement design. Weight-in-motion (WIM) sensors have become popular for weight measurements. A three-dimension glass fiber-reinforced polymer packaged fiber Bragg grating sensor (3D GFRP-FBG) is introduced for in-pavement WIM measurement at low speed. Sensitivity study shows that the sensor is very sensitive to the sensor installation depth and the loading position. The developed 3D GFRP-FBG sensor is applicable for most practical pavements and it also shows a very good long-term durability. Among the three components of the sensor, the longitudinal component has the highest sensitivity for WIM measurements. Field testing results indicated that the 3D GFRP-FBG sensor has a measurement accuracy of 90%, 79%, and 67% for longitudinal, transverse, and vertical components, respectively. Thus, it is recommended to use the longitudinal sensing unit if only one dimension of the sensor is to be further advanced for practice.

# ACKNOWLEDGEMENTS

Firstly, I would like to express my sincere gratitude to my advisor Dr.Ying Huang for the continuous support of my graduate study and related research, for her patience, motivation, and immense knowledge. Her guidance helped me in all the time of research and writing of this thesis. I could not have imagined having a better advisor and mentor for my Master study.

Besides my advisor, I would like to thank the rest of my thesis committee: Dr. Magdy Abdelrahman and Dr. Zhili" Jerry" Gao, for their insightful comments and encouragement.

I would also like to thank my parents, two elder brothers, elder sister and my little sister. They are always supporting me and encouraging me with their best wishes. Finally, I would like to thank my wife, Shaima' Almbaidin. She is always there cheering me up and stood beside me through the good times and bad.

# TABLE OF CONTENTS

# LIST OF TABLES

# LIST OF FIGURES

# LIST OF SYMBOLS

a........................................................length of pavement panel

b........................................................width of pavement panel

h........................................................thickness of pavement panel

$\mu$ ......................................................Poisson's ratio of pavement

E ......................................................modulus of pavement

k........................................................stiffness of subgrade

D........................................................flexural rigidity of plate

$\eta$ ......................................................transverse coordinate of tire center

$\zeta$........................................................longitudinal coordinate of tire center

$L_0$........................................................length of tire contact area

$B_0$........................................................width of tire contact area

$P(x,y)$................................................distribution of the contact pressure

P ......................................................compressive force of a single tire

PL......................................................linear load function

v........................................................average vehicle speed

$x_0$ ......................................................longitudinal coordinate of sensor center

$y_0$ ......................................................transverse coordinate of sensor center

$h_0$ ......................................................depth of sensor in the pavement

$\varphi$ ......................................................Strain transfer rate

$T_0$........................................................half duration of $P_L$

$t_0$...................................................... half effective duration of $S_L$

# 1. INTRODUCTION

## 1.1. Background

There are more than 4 million miles of roads in the United States [1]. Concrete pavements play an important role in the highway systems of United States during the past 60 years [2]. Concrete pavements can support heavy loads with less deformation than asphalt pavements, also serve longer life with little or no maintenance [2, 3]. Because of all these advantages, 160,000 miles of national highways at United States are using concrete pavements [2].

### 1.1.1. Concrete pavements

Figure 1 shows a typical cross section of the rigid pavement, also known as concrete pavement. Rigid pavements are placed either on the prepared sub-grade or on a single layer of granular or stabilized material. There is layer between the concrete and the subgrade, known as the sub-base course [4].
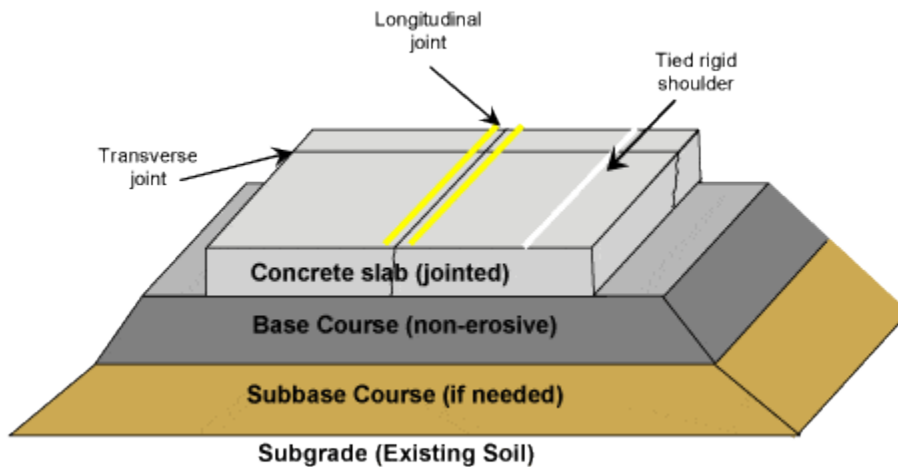


Figure 1. A typical cross section of the rigid pavement [5]

The surface layer of the rigid pavement is usually made up from Portland Cement Concrete (PCC), which is considered as the stiffest layer in rigid pavement and provides the majority of strength.  The base or sub-base layers are less stiff than the PCC surface but they play important role to keep the pavement safe from frost, also they contribute in pavement drainage and provide

1

a working platform for construction equipment. Rigid pavements are stiffer than flexible pavements due to the high modulus of elasticity of the PCC material (4,000,000 psi) [6], resulting in low deflection under loading. Usually, the plate theory can be used to analyze the rigid pavements. In order to handle the thermal stresses, rigid pavements can be reinforced by steel, which is generally used to reduce or eliminate joints and maintain tight crack widths [5].

From Figure 1, it can be seen that each structural component of the rigid pavement (PCC, base, and subgrade) would play a significant role on the performance of the rigid pavement. The stiffness of concrete would influence the pavement performance critically because the loads are transferred to the subgrade by the flexural strength of the pavement [4]. The pavement performance is strongly influenced by the underlying soil especially with respect to stability, bearing strength, consolidation, and moisture [3]. With the rigid pavement distributing loads wider and the effective layer structure, the pressure in the base and subgrade are low and can be supported sufficiently by the subgrade. However, for Weight-in-motion (WIM) measurement, the effect of base on the theoretical stress/strain analysis is usually neglected because of the short measurement period during the loading for weight-in-motion. More investigations for how the base and subgrade will influence the measurement accuracy of the WIM measurement is needed and will be performed in future study.

### 1.1.2. Stress distribution inside rigid pavement

The stress analysis of rigid pavements have long been a challenging problem for highway designers. The complexity of the vast multitude of variables to be considered has led to various approaches to analysis. The approaches to analyze the stress or strain distribution inside a rigid pavement under loads include theoretic or analytical analysis and numerical analysis.

The first analyses attempt of the stress distribution inside rigid pavement under loading was analyzed by Timoshenko [7] assuming the pavement section was in a bending as an elastic plate. Timoshenko [7] distinguished the difference of bending stresses in thin or thick plates and those in thin plates with small or large deflections. Because the concrete pavement is generally assumed as a thin plate, Kirchhoff bending plate theory has become common to analyze the stress and strain distribution in rigid pavements [8]. The assumptions of this theory include 1) the pavement plate uses homogenous, isotropic, and elastic material; 2) the cross section normal to the neutral axis remains plane before and after bending and there is no deformation along the thickness of plate. With these assumptions, the vertical bending stress, $\sigma_v$, equals to 0 at any point across the depth and the analysis becomes a problem with plane stress. In addition, the theoretic stress/strain distribution solution from these equations from this theory showed dependence on load condition and foundation types.

Generally, there are three types of foundations models are commonly used according to foundation types, including Winkler foundation, Pasternak foundation, and Kerr foundation. In a Winkler foundation, the subgrade was assumed to be composed of closely linear springs and subgrade shear strength was neglected. The subgrade reaction was proportional to the deflection. For a Pasternak foundation, the shear interaction between the spring elements was integrated and subgrade shear force was assumed to be proportional to the variation in deflection in the soil layer [8]. In a Kerr foundation, the subgrade was described with two spring constants along with presence of subgrade shear interaction [8]. Because of the simplicity and popularity of the Winkler foundation method in civil engineering, this study uses the Winkler foundation as a foundation type for theoretical analysis in Chapter 2 [8].

3

Using Winkler foundation, a complete theory of structural stress/strain analysis of rigid pavement was proposed by Westergaard [9] using the classical thin plate theory. Westergaard also assumed that the pavement plate used homogenous, isotropic, and elastic material. Based these assumptions, Westergaard introduced the stress in the three critical areas including interior, edge and corner of the pavement limiting the analysis to be only located in three locations [9].

In practice, sometimes, the analytical solutions for many of rigid pavements structures have become impossible to be obtained due to the complexities associated with geometry, boundary conditions, and material properties. Thus, in addition to theoretic or analytic analysis, numerical analysis is also very popular for stress and strain analysis of rigid pavements such as Discrete Element Method (DEM), Finite Element Method (FEM), and Finite Difference Method (FDM) [9].

In addition, rigid pavements are exposed to different types of stress, which would lead to early failure of the pavements, such as curling stress due to temperature, moisture, shrinkage, and loading from traffic. However, curling stresses are usually not considered in rigid pavement design because the curling effect is limited comparing to load repetitions, which are neglected in this study.

## 1.1.3. Vehicle weight effect on rigid pavement design

Estimation a traffic over the design period is one of key parameters in the rigid pavement design [10]. In other words, a controlling factor in rigid pavement design is to accurately estimate the vehicle axle loads that the pavement is expected to practice over its design life. The load from the vehicle is carried from the rigid pavement at three different location (interior, corner, and edge) as shown in Figure 2.
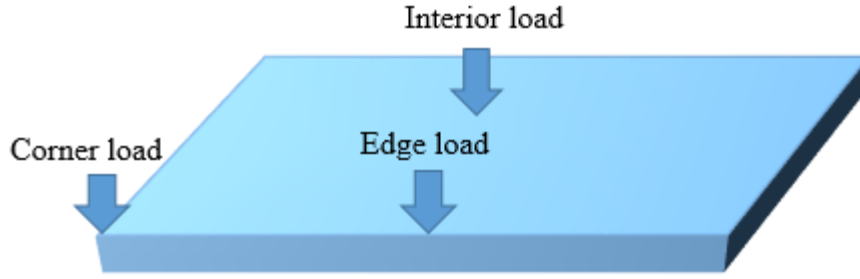
Figure 2. Corner, edge and interior loading

These loading will generate stresses, corner stress ($\sigma_c$) is associated with corner breaks, while interior ($\sigma_i$) and edge ($\sigma_e$) stresses are associated with mid-slab cracking [3]. The generated stresses inside rigid pavement from three loading location $\sigma_c$, are described as [11]:

$$\sigma_C = \frac{3P}{h^2}\left[1 - \left(\frac{\alpha\sqrt{2}}{\beta}\right)^{0.6}\right];$$

$$\sigma_e = \frac{0.572P}{h^2}\left[4\log_{10}\left(\frac{\beta}{\chi}\right) + 0.359\right];$$

$$\sigma_i = \frac{0.316P}{h^2}\left[4\log_{10}\left(\frac{\beta}{\chi}\right) + 1.069\right]. \tag{1}$$

where, h is the slab thickness in cm, P is the wheel load in Kg, $\alpha$ is the radius of the wheel load in cm, $\chi$ the radius of relative stiffness in cm and $\beta$ is the radius of the resisting section in cm.

Fatigue stresses are produced by the traffic load as described in Equation 1. Increasing in the weight of the vehicle will produce more fatigue stresses up to tens or hundreds of millions of repetitions for busy highways [3]. The philosophy that govern the rigid pavement design that it based upon the traffic loads alone when considering the pavement thickness [3], indicating the important of weight when designing the rigid pavement.

5

**1.1.4. Vehicle load long-term effects on rigid pavement**

As the continuous increase of traffic loads, the truck weight has become a more and more critical factor for the management of road networks, which impacts significantly on the road maintenance costs and the safety of road users [12]. Overloading on roads would result in increasing deterioration level of the pavement which could lead to early pavement failure [13], since the damage of the pavement increases the 4th degree of power of exponential geometrics as the increase of vehicle weight [14]. Also, the overloaded truck increases the risk of accidents [15]. To enforce the weight limit on roads to avoid overloading, weight measurement is required for most national highways and significant road sections worldwide.

Currently, stationary weight scales together with weight stations are still the major weight control facilities worldwide. These stationary weight scales have some limitations, such as time-consuming process for weight measurements which usually takes 5 minutes for each truck weight measurement, limited spaces (usually 15 trucks) for trucks to pass by [16], potentials for missing overloaded trucks [15], and accident hazards for stopped vehicles on the weight station entrance [17]. Thus, to overcome these disadvantages, in recent decades, weight-in-motion (WIM) technology has become popular for weight measurements for road networks.

**1.2. Weigh-in-Motion (WIM) Technology**

The basic principles of WIM technology were developed in the 1950s [18]. Currently, there are more than 1,000 operational WIM stations on the US highway system [19] and distributed as shown in Figure 3.

Figure 3. Operational WIM station in USA [20]

WIM defined as a process used to calculate the dynamic load applied in the road surface by the vehicle's tires for estimating the static weight of the vehicle. The WIM system consists of set of sensors and data collection and processing instruments. The sensors for WIM measurement are used to measure the dynamic weights of passing vehicles as an electrical signal. These data are transmitted to be processed by the instrument to convert it to a physical character which can be understood by the receiver, such as axle weight and gross weight. In general, there are two types of weigh-in-motion systems: low speed weigh-in-motion (LS-WIM) for passing speed of up to 25mph, and high speed weigh-in-motion (HS-WIM) for vehicle passing speed up to 80mph. Both of these appeared in late of 1960's [21]. Low speed WIM sensors are usually applied in combination with weight station which accelerates significantly for truck weight measurements, and high speed WIM sensors are applied in roads directly to collect weight information for traffic managements such as traffic rule enforcement. According to American Society for Testing and Materials (ASTM) [22], many of data items could be produced by WIM system, such as wheel load, axle load, axle-group load, gross vehicle weight, speed, center-to-center spacing between

7

axles, vehicle class (via axle arrangement), site identification code, lane and direction of travel, date and time of passage, sequential vehicle identification number, wheelbase (front-most to rear-most axle) and equivalent single-axle loads (ESALs).

## 1.3. Existing Technologies for Weigh-in-Motion

For WIM measurements at low speed, there are several in-pavement sensors to be considered, including piezoelectric sensor, bending plates, load cells, and fiber optic sensors [23]:

1) Piezoelectric sensor: The piezoelectric sensor usually is encapsulated in an epoxy-filled metal channel, such as aluminum as shown in Figure 4. It is placed in the travel lane perpendicular to the direction of travel enabling the wheels of one axle to hit the sensor at the same time. When a load is applied to the piezoelectric material, an electrical charge is produced. The load is transferred through the pavement then to the sensor which is embedded in the pavement. By measuring and analyzing the charge produced, the sensor can be used to measure the weight of a passing tire or axle group [23].
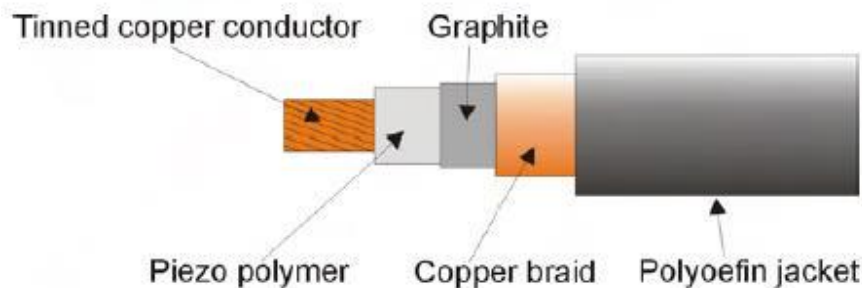


Figure 4. Typical piezoelectric sensor [24]

2) Bending plate scale: A bending plate scale contains of two steel plates placed close to each other in an appropriate distance to cover a lane. The strain gages is attached on the steel plates at critical points to measure the generated strains through the plate as a tire passing over. Then the measured strains are analyzed to determine the axle load. Figure 5 shows the bending plate scale components and the installation scene [23].
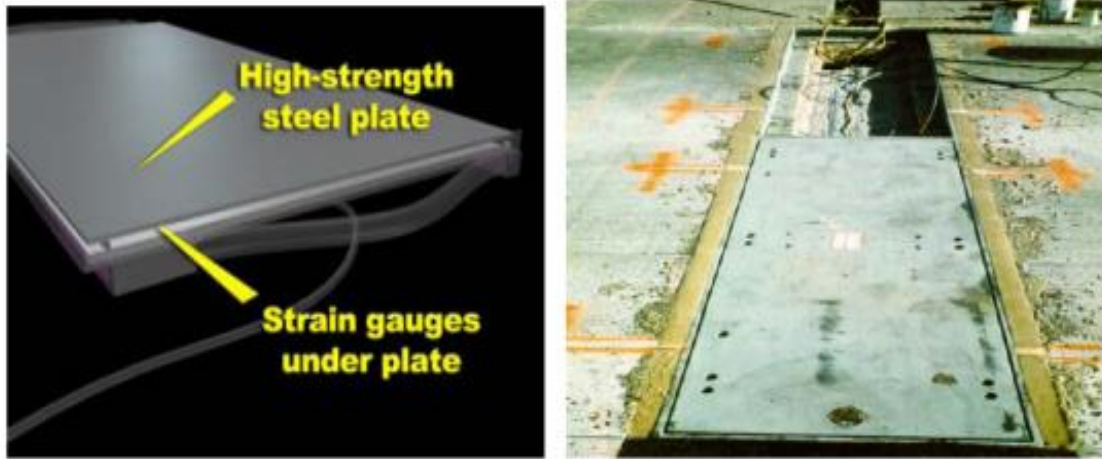
Figure 5. Bending plate scale [23]

3) Load cell: A single load cell scale contains of two weighing plates with a surface size of 6 ft. by 3 ft. 2 in., placed close to each other to fully cover a normal 12 ft. traffic lane. A single hydraulic load cell is installed at the center of each platform as shown in Figure 6 to measure the force applied to the plate. The load measurements are recorded and analyzed to measure tire and axle loads [23].
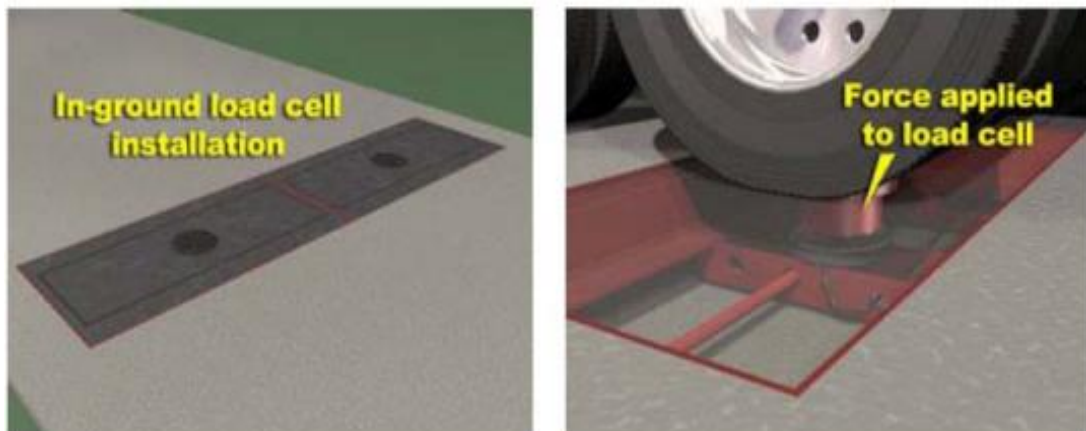


Figure 6. Load cell [23]

These sensors (piezoelectric sensor, bending plate scale and load cell) generally show inversely proportional cost and accuracy characteristics. Table 1 compares the cost, accuracy, sensitivity, and life cycle for the common type of sensor embedded in a WIM system. In addition,

9

these electrical sensors (Piezoelectric sensor, Bending plate and Single load cell) showed a dramatic effect from the surrounding environment, such as moisture. It also has some disadvantages such as high electromagnetic interferences (EMI), high cost and relatively short life cycle with a moderate reliability and accuracy, and a long time for traffic shut-down to install the sensors within the road.

Table 1. WIM sensor comparison [25-27]

|  | Piezoelectric sensor | Bending plate | Single load cell | Optic fiber sensor (FBG) |
|---|---|---|---|---|
| Annual life cycle cost | Low ($ 5,000) | Medium ($ 6,000) | High ($ 8,000) | Low ($ 1,000) |
| Accuracy | +/- 15% | +/- 10% | +/-6% | +/- 10% |
| Sensitivity | High | Medium | Low | High |
| Expected life | 4 years | 6 years | 12 years | >15 years |

## 1.4. Fiber Optic Sensors for WIM Measurements

The Fiber Optic Sensors (FOS) have become acceptable in the vast field of civil engineering because of its unique features. Table 1 shows that fiber optic sensor is a potential solution for cost-effective WIM measurements, especially at low speed, due to their advantages of small size, light weight, immunity to electromagnetic interference, capability to serve in harsh environments such as high temperature, corrosion and humidity, high sensitivity [28], and higher accuracy [29].

Among various fiber optic sensors, one of the most widely used sensors is fiber Bragg grating (FBG) sensor. The FBG was firstly formatted in an optical fiber in 1978 at the Canadian Research Centre, Ottawa, Canada [30]. The FBG has all the advantages of a fiber optic sensor and it has its unique property of good resolution and ability to be multiplexed [25, 26]. Also, a single FBG sensor could potentially provide a lot of traffic and road characteristics, such as weight-in-motion, vehicle speed, classification, road fatigue, temperature and traffic signal vehicle detection.

All of these features contribute in extending the system's durability and driver safety [31]. Hence, it can be a potential solution for long-term WIM system and it has been tested for such application as follow:

1) Wang et al [32] stated that the experimental results for WIM measurement based on FBG sensor installed on steel plates instead of bridge beam showed a good repeatability and reliability;

2) Moyo et al [33] demonstrated that the FBG sensor could be used to assess traffic loading on bridges;

3) Berardis et al [34] indicated that a WIM system based on FBG sensors is good for high-speed road vehicle and high load resolution;

4) Cass et al [35] showed that FBG sensors could be used to monitor internal and external factors on roads such as vehicle speed and its weight;

5) Udd et al [36] stated that a single FBG sensor is effective to monitor vehicle speed, weight-in-motion, and vehicle classification and because of its high sensitivity, by installing the FBG sensor on a bridge, it can detect people standing on a bridge.

However, since FBG sensors are made up by glass fiber, they are very easy to be damaged when installing inside pavements for WIM measurements and it requires appropriate packaging before installation. On the other hand, glass fiber reinforced polymer (GFRP) material has become widely accepted for use in civil engineering applications as a viable option to replace steel [37], which can be a potential solution to package FBG to improve its ruggedness [38, 39]. In this thesis, we will systematically investigate   a GFRP packaged FBG sensor for WIM measurements at low speed.

## 1.5. Problem Statement and Significance of This Study

From the above literature review, it is clear seen that the truck weight has become a more and more critical factor for the management of road networks, which impacts significantly on the road maintenance costs and the safety of road users. Thus, it is necessary to enforce the weight on most of our national roads to prevent overloading vehicles from deteriorating the road surfaces. The stationary weight scale is the most common weight scale used worldwide, but the stationary weight scale has limited space, which may induce traffic jam where truck traffic is significant and may miss heavy weight trucks, leading to new technology development for weight measurement in motion, known as WIM technique.

Currently, there are four types of in-pavement sensors which can be used for WIM measurements, including piezoelectric sensor, bending plate scale, load cell, and FBG sensor. Among these sensors, the electrical sensors such as piezoelectric sensor, bending plate scale, and load cell, share the common disadvantages of high electro-magmatic interference (EMI), high cost and relatively short life cycle with a moderate reliability and accuracy, and a long time for traffic shut-down to install the sensors within the road. On the other hand, the FBG sensors have unique advantages of small size, high sensitivity, and high accuracy make it a good candidate for long-term WIM measurement.

However, bare FBG sensor which is made up by glass material is very weak without packaging, which is not practical for applications inside pavements with harsh construction process. Thus, there is an urgent need to develop a robust packaging method for FBG sensors to measure WIM in a long term and reliable manner. The development of this robust and reliable FBG sensor will in return provide the transportation agency an alternative for effective and long-term WIM measurements.

**1.6. Objectives and Organization of This Thesis**

In this study, the main objective is to develop an effective GFRP packaged FBG sensor for robust long-term WIM measurements. To achieve this objective, this study identifies four specific tasks which can be summarized as follow:

1) Develop the GFRP-FBG sensor for WIM measurements theoretically;

2) Perform sensitivity study of the sensor on several key parameters, such as sensor depth, panel size, load coordination, and panel material property on the sensitivity of the GFRP-FBG sensor for the WIM measurements;

3) Investigate the long-term performance of the developed WIM sensor;

4) Validate the developed sensor for WIM measurement through field testing of case study.

This thesis is thus organized as follows: in Chapter 1, an introduction of weight-in-motion and a detail literature review are provided; in Chapter 2, the operational principle of FBG sensor and the geometric design of the GFRP-FBG WIM sensor are introduced ; in Chapter 3, the transfer function of the GFRP-FBG sensor for WIM measurements is derived; in Chapter 4, a sensitivity study of controlling factors on the sensitivity of the sensor and an evaluation of the developed sensor for long term durability are performed; in Chapter 5, field testing of case study is performed to validate the theoretical study performed in Chapter 3;  and in Chapter 6, conclusion and future work have been presented based on the findings from this study.

## 2. SENSOR DESIGN AND CONFIGURATIONS

Glass Fiber Reinforced Polymer Fiber Bragg Grating (GFRP-FBG) sensor has been selected to be used for WIM measurement in rigid pavements. In this chapter, the operational principle of the FBG sensor and the geometric design of the GFRP-FBG sensor are introduced in detail.

### 2.1. Operational Principle of FBG Sensors

An FBG is made by shedding a periodic pattern of intense ultraviolet UV in order to expose the core of single mode fiber, creating a refractive index modulation so called grating. Bragg wavelength formed due to reflected light from the periodic refraction change [38] which can be descried as:

$$\lambda = 2n\Lambda \tag{2}$$

where, n is the effective index of refraction and $\Lambda$ is the grating periodicity of the FBG. Bragg wavelength depends on the Brag condition and the wavelength at which this reflection occurs. Light signals at wavelengths other than the Bragg wavelength pass through and only the wavelength matched with Bragg wavelength will be reflected. Figure 7 shows a schematic of the operational principle of a FBG sensor.

Due to temperature and strain dependence of the grating period, $\Lambda$, the Bragg wavelength will change as function of temperature, T, and strain, ε. The strain-Bragg wavelength relationship for the FBG can be described as [38]:

$$\varepsilon = \frac{1}{(1-P_e)}(\frac{\Delta\lambda}{\lambda} - \frac{\Delta\lambda_{Te}}{\lambda_{Te}}) \tag{3}$$

where $P_e$ is the optical elasticity coefficient of the optic fiber, $\lambda$ is the center wavelength from the FBG strain sensor, and $\lambda_{Te}$ is the measured center wavelength from the FBG temperature

compensation sensor. Since the strain in pavement can be directly related to the vehicle weight, P, loaded on the pavement, the FBG sensors, thus, can be used for WIM measurements.
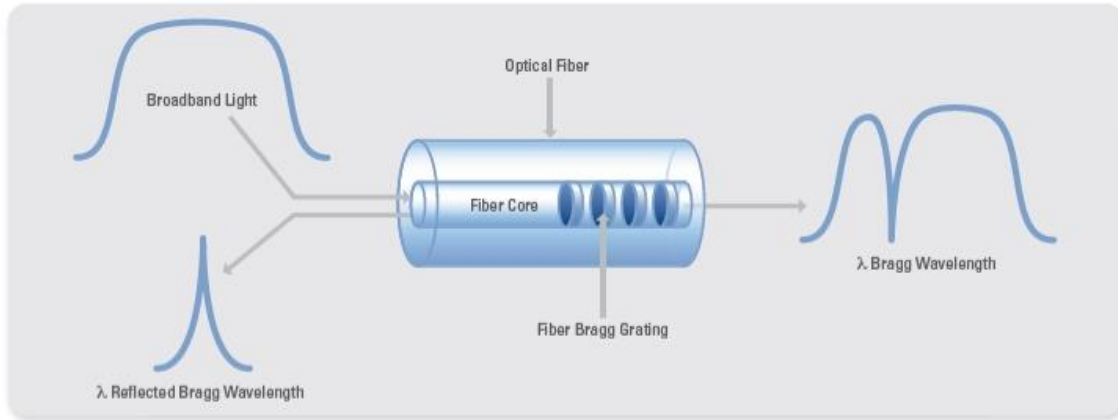


Figure 7. The operational principle of a FBG sensor [40]

## 2.2. GFRP-FBG Sensor Geometric Design

The GFRP-FBG sensor previously developed by Zhou et al and Zhang et al [38, 39] will be used as the sensing unit for the WIM measurements in this thesis. Figures 8 (a~c) show the geometric design for the GFRP-FBG sensor. The GFRP-FBG sensor has three components in three dimension (3D), one in longitudinal direction, one in transverse, and one in vertical direction. The short gauged component is aligned in vertical direction, which intends to detect the vertical strain while the long gauged components are used to detect the longitudinal and transverse strains. The longitudinal and transverse sensing components of the 3D GFRP-FBG sensor were designed with 2.2 in (56mm) in length and the vertical component had a height of 2.1 in (53 mm) including the length of the GFRP holder. All the 3D GFRP-FBG sensor components shared the same diameter of 0.2 in (5mm). Also, the GFRP-FBG sensor has a strain sensitivity of $7.937 \times 10^{-7}$ nm/$\mu\varepsilon$, which is (1-$P_e$) term in Equation 3.
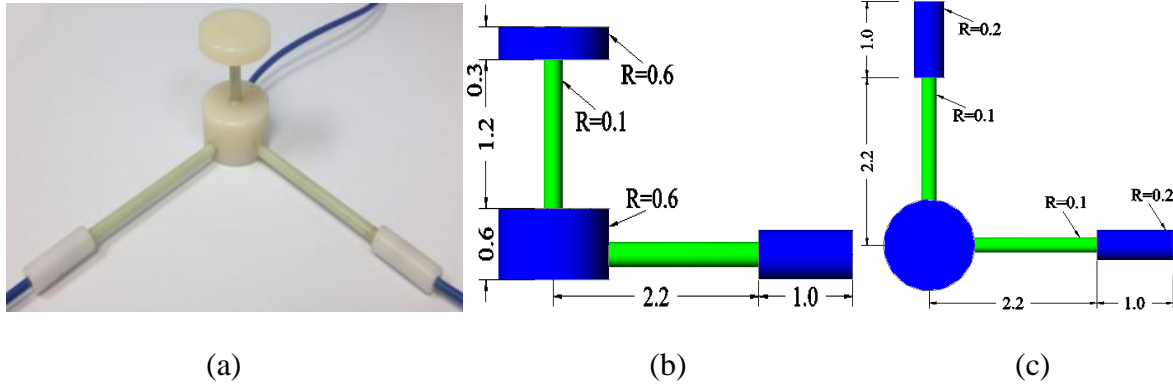
Figure 8. Geometric design of the 3D GFRP-FBG sensor: (a) Photo of the 3D GFRP-FBG sensor, (b) Elevation view, and (c) Plan view (Unit: in.)

## 2.3. Summary

In this Chapter, the operational principle of FBG sensor and the geometric design of GFRP-FBG sensor are described. FBG sensor is used as a strain sensor. The generated Bragg wavelength changes of the FBG sensor depends on the strains on the grating and the strains can be directly related to the applied load (vehicle weight) on pavement, thus, for WIM measurements. To measure the WIM through embedded FBG sensors inside pavements, GFRP is used as packaged material in this study. The GFRP packaged FBG WIM sensor contains of three components, one in longitudinal direction, one in transverse, and one in vertical direction and it has a strain sensitivity of $7.937 \times 10^{-7}$ nm/$\mu\varepsilon$ which will be related to the WIM sensitivity in next chapter.

16

# 3. GENERAL THEORETICAL ANALYSIS ON SENSOR SENSTIVITY

After the geometric design of the GFRP-FBG sensor for in pavement WIM measurements, this chapter derives the transfer function of the GFRP-FBG sensor for WIM measurement at low speed using the convolution principle between load function and the sensor's sensitivity function. Figure 9 shows a flow chart for the process to develop the transfer function of the GFRP-FBG sensor for WIM measurement. The weight transfer function is derived for GFRP-FBG sensor by assuming that the sensor is embedded inside thin rigid pavement, the strains in longitudinal and transverse directions are obtained by applying the elasticity theory. The strain in vertical direction is obtained by assuming the plate as a homogenous plate under plane stress, then, the weight transfer function of the sensor's components is the result of the combination between strain formulas and strain-wavelength relationship (Equation 3). Details will be further introduced in this chapter.
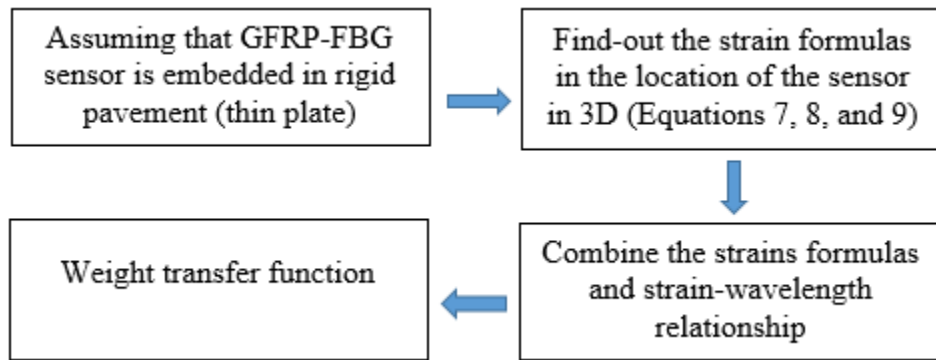
Figure 9.Procedure to develop the weight transfer function of GFRP-FBG sensor

## 3.1. Strain Signal Generation

When a vehicle passes on the road, the pavement produces strain signals which will be picked up by wavelength changes of the embedded GFRP-FBG sensor as shown in Equation 3. The strain signal inside the pavement is formed from the convolution of the load from the tire contact area and the sensitivity function of the embedded sensor [41]. Theoretically, for a specific

tire with contact pressure of $P(x,y)$ at a location $(x,y)$ inside the contact area with length of $L_o$ and width of $B_o$, the contact pressure as shown in Figure 10(a) is [41]:

$$P = \int_{L_0 \times B_0} p(x, y)ds .$$  (4)

If the embedded GFRP-FBG sensor has a strain sensitivity function, $S_L(t)$, along the length of the sensor as shown in Figure 10(a), the strain signal, $I(t)$, as shown in Figure 10(b) can be obtained as [41]:

$$I(t) = \int_{-\infty}^{+\infty} P_L(t - \tau)S_L(\tau)vd\tau .$$  (5)



(a)                                    (b)
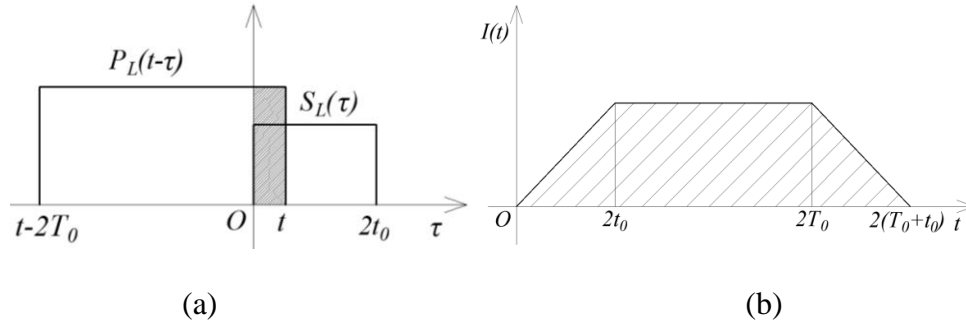
Figure 10. Operation to acquire the GFRP-FBG sensor's strain signal by convolution (a) and (b) strain signal [41]

## 3.2. Load Function

The load function along the wheel path within the contact area $(L_0 \times B_0)$ is a constant value at travelling speed $v$. The contact pressure $P_L(t)$ in Equation 5 become:

$$p_L(t) = \frac{P}{L_O} \Pi\left( \frac{t - T_0}{2T_0} \right)$$  (6)

## 3.3. Sensitivity Function

Assuming the GFRP-FBG sensor is embedded inside a pavement panel with a length of $a$ and a width of $b$. The contact pressure area of length $u_0$ and width $v_0$ is centred at $(\zeta, \eta)$ on the

18

concrete panel surface as shown in Figure 11. Based on the thin plate theory, the vertical displacement inside the pavement is as follow [41]:

$$w(x, y) = \frac{16P}{\pi^2 u_0 v_0} \sum_{m=1}^{\infty} \sum_{n=1}^{\infty} \frac{1}{mn[\pi^4 D(\frac{m^2}{a^2} + \frac{n^2}{b^2})^2 + k]} \sin \frac{m\pi x}{a} \sin \frac{n\pi y}{b} \sin \frac{m\pi \xi}{a} \sin \frac{n\pi \eta}{b} \sin \frac{m\pi u_0}{2a} \sin \frac{n\pi v_0}{2b} \quad (7)$$
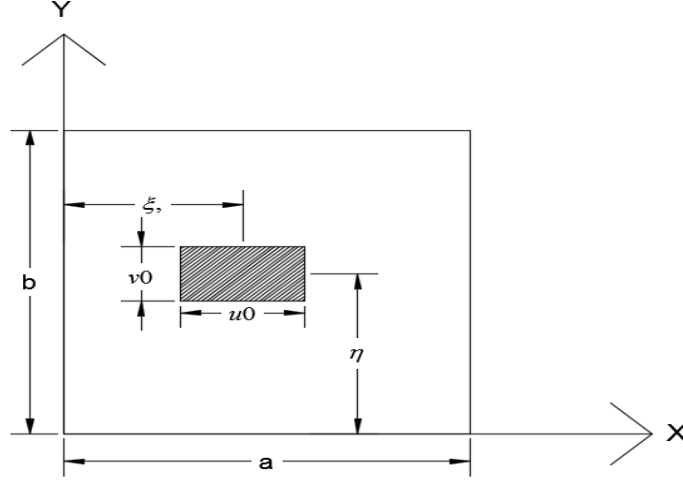


Figure 11. Pavement panel under partial uniform load

where, P is the force on the pavement panel which is corresponding to the weight of the passing vehicle, which is the integration of the pressure q within the loading area $u_0 \times v_0$, m and n are the summation variables.

Considering that x direction is the longitudinal direction of the 3D GFRP-FBG sensor which is parallel to the wheel path, y direction is the transvers direction of the sensor which is perpendicular to the wheel path, we can obtain the strains in longitudinal and transverse directions of the pavement through applying the theory of elasticity based on Equation 7 as follows:

$$\varepsilon_L = -z \frac{\partial^2 w}{\partial x^2} = \frac{16Pz}{u_0 v_0 a^2} \sum_{m=1}^{\infty} \sum_{n=1}^{\infty} \frac{m}{n[\pi^4 D(\frac{m^2}{a^2} + \frac{n^2}{b^2})^2 + k]} \sin \frac{m\pi x}{a} \sin \frac{n\pi y}{b} \sin \frac{m\pi \xi}{a} \sin \frac{n\pi \eta}{b} \sin \frac{m\pi u_0}{2a} \sin \frac{n\pi v_0}{2b} \quad (8)$$

$$\varepsilon_{Tr} = -z \frac{\partial^2 w}{\partial y^2} = \frac{16Pz}{u_0 v_0 b^2} \sum_{m=1}^{\infty} \sum_{n=1}^{\infty} \frac{n}{m[\pi^4 D(\frac{m^2}{a^2} + \frac{n^2}{b^2})^2 + k]} \sin \frac{m\pi x}{a} \sin \frac{n\pi y}{b} \sin \frac{m\pi \xi}{a} \sin \frac{n\pi \eta}{b} \sin \frac{m\pi u_0}{2a} \sin \frac{n\pi v_0}{2b} \quad (9)$$

19

Assuming the pavement panel is an isotropic thin plate under plane stress and the modulus of the elasticity of the host material is E, then the strain in vertical direction could be provided as follows:

$$\varepsilon_V = -\frac{P}{L_0 B_0 E} - \frac{\upsilon}{1-\upsilon}(\varepsilon_L + \varepsilon_{Tr}) \tag{10}$$

Thus, the strain transfer function of the sensor can be obtained by combining Equations 3, 8, 9, and 10 and the strain transfer rate of the GFRP to concrete, φ, [38] which is related to the modulus of the elasticity of the host material, E, following the reference by Zhou et al [38]. The transfer function of the GFRP-FBG sensor for WIM measurement in three directions (longitudinal, transverse, and vertical direction), thus, can be represented as below:

$$P = A_L\left(\frac{\Delta\lambda_L}{\lambda_L} - \frac{\Delta\lambda_{Te}}{\lambda_{Te}}\right) = A_T\left(\frac{\Delta\lambda_{Tr}}{\lambda_{Tr}} - \frac{\Delta\lambda_{Te}}{\lambda_{Te}}\right) = A_V\left(\frac{\Delta\lambda_V}{\lambda_V} - \frac{\Delta\lambda_{Te}}{\lambda_{Te}}\right) \tag{11}$$

in which, $\lambda_L$, $\lambda_{Tr}$, $\lambda_V$, and $\lambda_{Te}$ are the measured centre wavelengths from longitudinal, transverse, vertical components of the 3D GFRP-FBG sensor and the temperature compensation sensor, respectively. The $A_L$, $A_T$, and $A_V$ are the weight sensitivity of the GFRP-FBG sensor for WIM measurements in longitudinal, transverse, and vertical directions, respectively and they can be represented as follows:

$$A_L = \frac{u_0 v_0 a^2}{16 z \varphi(1-P_e)\sum_{m=1}^{\infty}\sum_{n=1}^{\infty}\frac{m}{n[\pi^4 D(\frac{m^2}{a^2}+\frac{n^2}{b^2})^2 + k]}\sin\frac{m\pi x}{a}\sin\frac{n\pi y}{b}\sin\frac{m\pi\xi}{a}\sin\frac{n\pi\eta}{b}\sin\frac{m\pi u_0}{2a}\sin\frac{n\pi v_0}{2b}} ;$$

$$A_{Tr} = \frac{u_0 v_0 b^2}{16 z \varphi(1-P_e)\sum_{m=1}^{\infty}\sum_{n=1}^{\infty}\frac{n}{m[\pi^4 D(\frac{m^2}{a^2}+\frac{n^2}{b^2})^2 + k]}\sin\frac{m\pi x}{a}\sin\frac{n\pi y}{b}\sin\frac{m\pi\xi}{a}\sin\frac{n\pi\eta}{b}\sin\frac{m\pi u_0}{2a}\sin\frac{n\pi v_0}{2b}} ;$$

$$A_V = -\frac{L_0 B_0 E}{1-P_e} - \frac{\upsilon}{1-\upsilon}(A_L + A_{Tr}). \tag{12}$$

20

Therefore, the sensitivity of the 3D GFRP-FBG sensor in three dimensions can be analysed according to Equation 12 for WIM measurements at a vehicle driving speed up to 25 mph. If higher speed is presented, dynamic effect may occur and further investigation is required for the influence of the higher speed on the accuracy of the WIM measurements using the developed sensors.

From Equation 12, it can be seen that the WIM measurements sensitivity will be affected by several key parameters including sensor installation depth ($h_0$), pavement panel length and width, $a$ and $b$, property of the host material, the coordination of the wheel path on the pavement, $\zeta$ and $\eta$. The sensitivity of the sensor's performance on these parameters for WIM measurements will be further evaluated in Chapter 4 in detail.

## 3.4. Dynamic Range

The range of input signals that results in a meaningful output for the sensor is the dynamic range of the sensor. The dynamic range for 3D FBG-GFRP sensor could be calculated in terms of weight under the maximum load condition the 3D FBG-GFRP sensor or the host material can handle. Since the 3D FBG-GFRP sensor needs to stay within the elastic range, then the maximum stress could be handled from the 3D FBG-GFRP sensor is equal to yield strength of the GFRP material or host material whichever is less. The maximum stress yields to maximum strain in elastic zone Hook's law:

$$\varepsilon_{\max} = \frac{\sigma_{yield}}{E} \tag{13}$$

The dynamic range ($P_{\max}$) in terms of weight could be derived by substituting $\varepsilon_{\max}$ into Equation 3 to get $\Delta\lambda_{l\text{-max}}$, $\Delta\lambda_{T\text{-max}}$ and $\Delta\lambda_{v\text{-max}}$ maximum wavelength changes of the GFRP-FBG sensor for WIM measurements in longitudinal, transverse, and vertical directions, respectively. Then substitute $\Delta\lambda_{l\text{-max}}$, $\Delta\lambda_{T\text{-max}}$ and $\Delta\lambda_{v\text{-max}}$ into Equation 11, and it can be represented as follows:

$$P_{\max} = A_L \left( \frac{\Delta\lambda_{L-\max}}{\lambda_L} - \frac{\lambda_{Te}}{\lambda_{Te}} \right) = A_{Tr} \left( \frac{\Delta\lambda_{T-\max}}{\lambda_T} - \frac{\lambda_{Te}}{\lambda_{Te}} \right) = A_L \left( \frac{\Delta\lambda_{V-\max}}{\lambda_V} - \frac{\lambda_{Te}}{\lambda_{Te}} \right) \tag{14}$$

## 3.5. Summary

In this Chapter, the weight sensitivity function of the GFRP-FBG sensor and the dynamic range for all the sensor's component are derived. The weight sensitivity function is derived for the three components of GFRP-FBG sensor by assuming that the sensor is embedded inside a thin rigid pavement panel. The vertical displacement of the panel is introduced from thin plate theory. The strains in longitudinal and transverse directions of the pavement are obtained through applying the theory of elasticity, and the strain in vertical direction is obtained by assuming the panel as an isotropic thin plate under plane stress. In addition, the dynamic range of the GFRP-FBG WIM sensor is also derived in this chapter from the maximum strain can the host material (concrete in this case) handle. Further sensitivity study for the key parameters which affect the weight measurement sensitivity of the GFRP-FBG WIM sensor will be put forward in next chapter.

# 4. SENSITIVITY STUDY

This chapter further performs a sensitivity study of the GFRP-FBG sensor for WIM measurements at any situation that the sensor could be embedded inside a rigid pavement. From Equations 11 and 12, the factors which could potentially affect the GFRP-FBG sensor's performance include sensor installation depth ($h_0$), pavement panel length and width, $a$ and $b$, property of the host material, the coordination of the wheel path on the pavement, $\zeta$ and $\eta$, and the long-term performance of the sensor. Thus, this section systematically investigates the influences of all these parameters on the GFRP-FBG sensor for WIM measurements.

## 4.1. Sensor Installation Depth, z

Theoretic analysis on the sensitivity of the sensor installation depth is performed using Equation 12 by changing the installation depth, z, and fixing the other parameters. Figures 12 (a~c) show the changes of the WIM measurement sensitivity with the sensor installation depth for the GFRP-FBG sensor's longitudinal, transverse and vertical component, respectively. As can be seen from Figure 12, the sensor installation depth influences significantly on the sensor's behaviour for the WIM measurement. If installed in the middle depth of the pavement panel, the sensor would not respond to any loading on top of the pavement. On the other hand, if installed at the bottom or the top of the pavement depth, the sensor would achieve its maximum WIM measurement sensitivity. Since an installation of the sensor on the top of the pavement panel is not practical in most cases, it is recommended to install the sensor at the bottom of the pavement panel for a maximum WIM measurement sensitivity. In addition, when comparing Figure 12(a), (b), and (c), it is obvious that the longitudinal component of the GFRP-FBG sensor has the largest WIM measurement sensitivity, which is three times bigger than that in transverse direction. The vertical component yields the smallest WIM measurement sensitivity due to the high stiffness of the

pavement panel. Therefore, for WIM measurements, sensors in longitudinal directions will provide the most sensitive measurement behaviour than the other two directions.
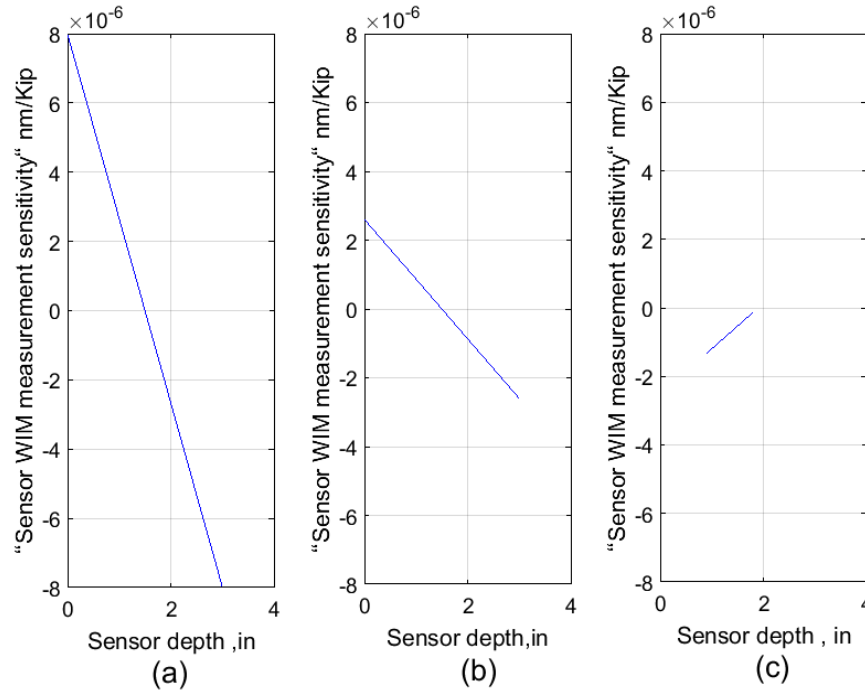


Figure 12. Sensor's WIM measurement sensitivity changes with sensor depth in (a) longitudinal, (b) transverse, and (c) vertical direction

## 4.2. Pavement Panel Size, a and b

Analysis on the sensitivity of the pavement panel size is performed using Equation 12 by changing panel length, *a* or *b*, and fixing the other parameters. Assuming a rectangular pavement panel with panel length equals to panel width, Figure 13 illustrates the WIM measurement sensitivity change of the GFRP-FBG sensor with the panel length for its longitudinal, transverse, and vertical components. In general, the WIM measurement sensitivity of the GFRP-FBG sensor is not very sensitive on the pavement panel size when compared with sensor installation depth. It also shows that smaller pavement panel will yield a larger WIM measurement sensitivity for the sensor. If the pavement panel has a size larger than 6ft (72 in), the GFRP-FBG sensor will not be influenced by the changes of panel length any more. In practice, most rigid pavements have a panel

24

length larger than 6ft, indicating the effectiveness of the developed sensor for WIM measurement in most rigid pavements.
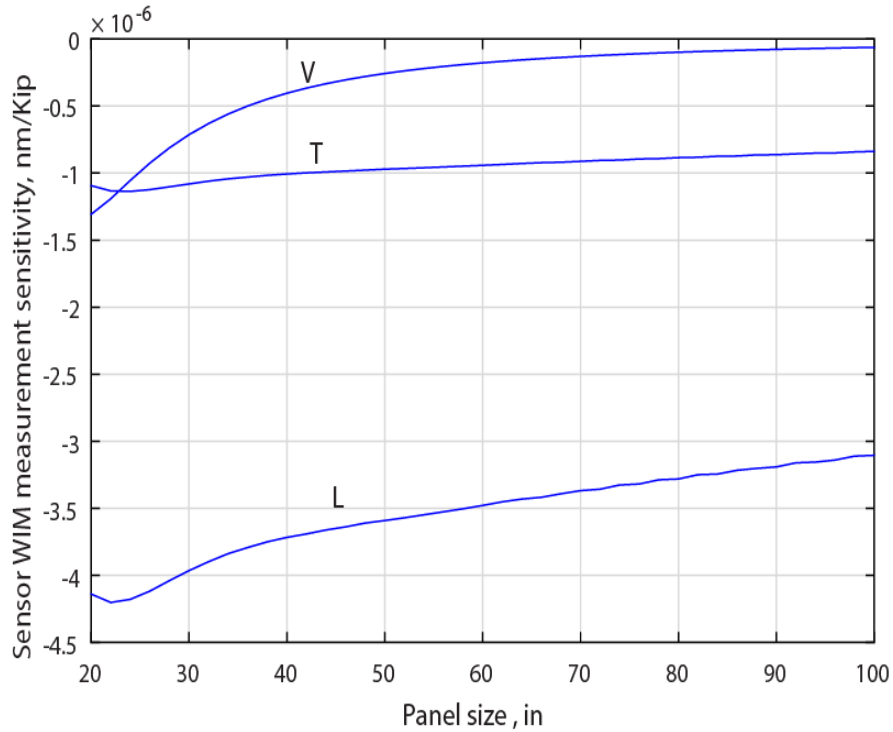


Figure 13. Sensor's WIM measurement sensitivity changes with pavement panel length in longitudinal (L), transverse (T) and vertical (V) directions

### 4.3. Longitudinal Location of the Wheel Load, ζ

It is important to know the location where the sensor starts to be sensitive to the WIM measurement for passing vehicle on the wheel path. This section investigates how the sensor performs as the vehicle moving along the wheel path in the longitudinal direction, ζ. Figures 14 (a~c) show the WIM measurement sensitivity changes of the GFRP-FBG longitudinal, transverse, and vertical components with the longitudinal location of the wheel load. The longitudinal component of the GFRP-FBG sensor has a significantly larger WIM sensitivity over the other two components. The longitudinal component of the 3D sensor produces a positive strain to the passing vehicle before the vehicle approaching the sensor and changes to a negative strain when the passing

vehicle drives within 12 inches (one foot) of the sensor location. If both positive and negative strains are counted for the WIM sensitivity, the longitudinal component of the 3D WIM sensor will increase 12.5%.



Figure 14. Sensor's WIM measurement sensitivity changes with longitudinal location of the wheel in (a) longitudinal, (b) transverse, and (c) vertical direction

### 4.4. Transverse Location of the Wheel Load, η

When a vehicle is driving on roads, it may not always stay on the wheel path. Therefore, it is critical to investigate how the sensor's accuracy changes with the loading location in transverse direction, η, if the vehicle is not exactly loaded on top of the sensor. Figures 15(a~c) show the WIM measurement sensitivity changes of the GFRP-FBG longitudinal, transverse, and vertical components with the transverse location of the wheel load. For the longitudinal component of the 3D sensor, if a WIM measurement accuracy of 80% is required, the centre of the wheel is required to be passing within 6 inches around the sensor to be effective. For the transverse component, it yields a similar loading range. For the vertical component, the vehicle needs to pass exactly on top

26

of the sensor to achieve an effective measurement. If the sensor is used in a weight station, some surface mark should be provided on the pavement panel to guarantee that the wheel passes exactly on top of the vertical component of the sensor and within 6 inches around the longitudinal or transverse components to achieve an accurate measurement.



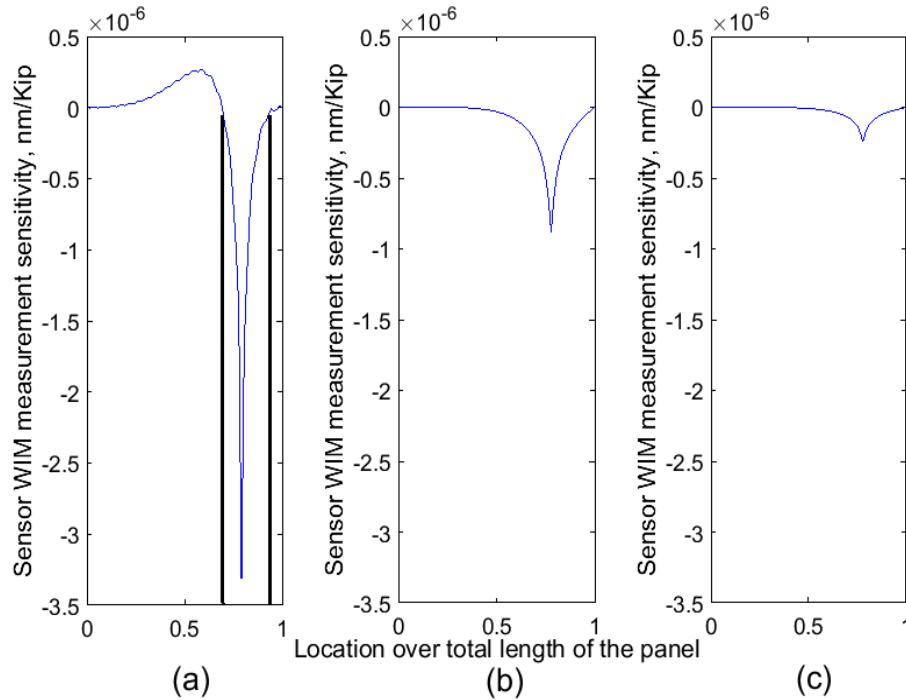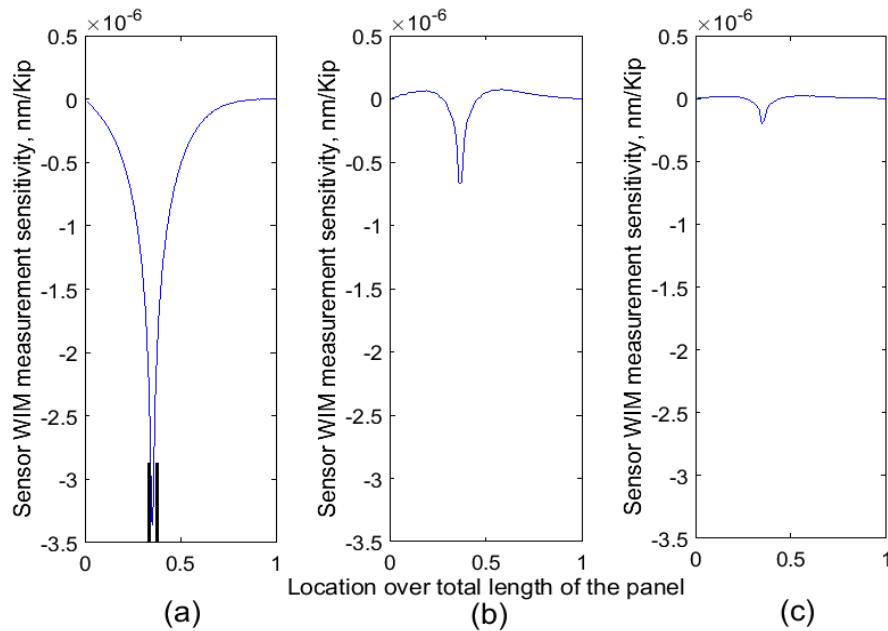Figure 15. Sensor's WIM measurement sensitivity changes with transverse location of the wheel in (a) longitudinal, (b) transverse, and (c) vertical direction

In addition, one axle of a truck may have two single tires or two dual tires. If a truck has two single tires in one axle, from Figure 15, with significant distance between the two tires in one axle, it can be seen that the sensor will not be influenced by the other tire of the axle and measures only the wheel load of one tire. However, if a truck axle has two dual tires, the sensor's response on the WIM measurement of one wheel will be affected by the neighbour tire and the influence depends on the space between the dual tires. Figure 15 also describes the influence of the neighbour tires on the measurement for the measured wheel. In case of dual tires, if the width of the tire is 21 inches and the space between the dual tires is 13.75 inches, the influence from the neighbour tire

on the measured tire is 3% of the total measurement, which can be neglected. Thus, for a truck axle with two dual tires, two sensors are required to measure the axle weight of the vehicle.

## 4.5. The Modulus of Elasticity of the Pavement, MOE

In practice, the sensor may be embedded in various types of host materials, for instance, if rigid pavement is used, the concrete may have various grades which may also affect the sensor's performance. Figure 16 shows the WIM measurement sensitivity change of the GFRP-FBG sensor's longitudinal, transverse, and vertical components with the change of modulus of elasticity (MOE) of the pavement panel's materials. The sensor's WIM measurement sensitivity will decrease with the increase of the MOE of the embedded host materials. If the MOE increases twice, the sensitivity of the sensor for all the three components will decrease almost half for the WIM measurement. Thus, for a more sensitive WIM measurement, a smaller stiffness of the host material is recommended for the GFRP-FBG sensor.
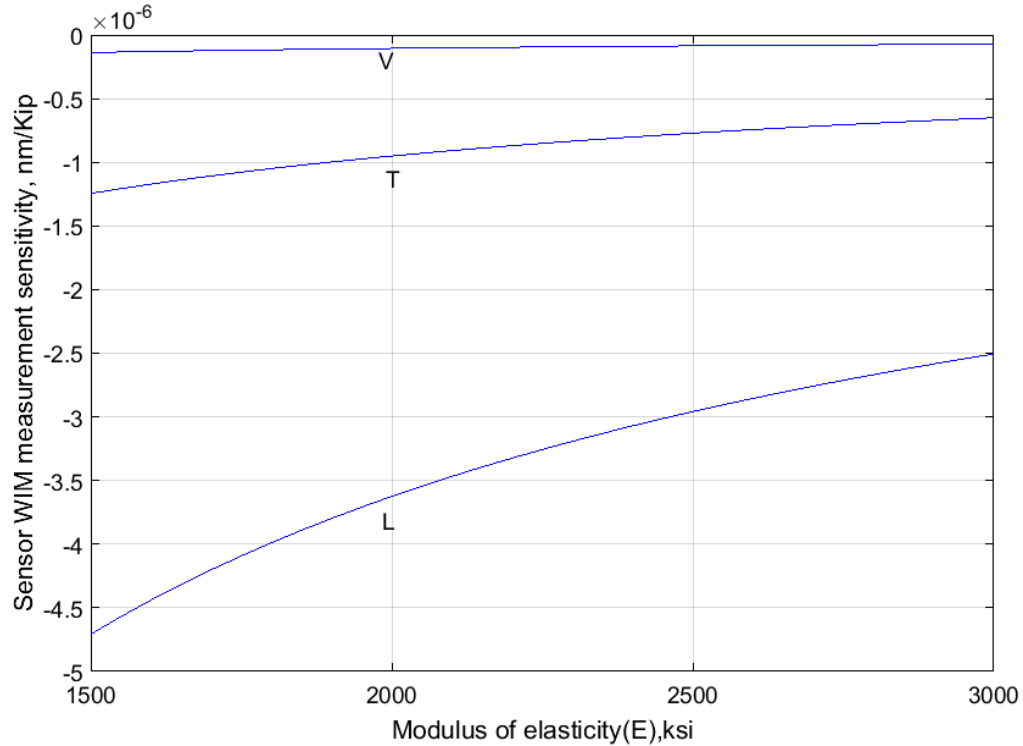
Figure 16. Sensor's WIM measurement sensitivity changes with pavement modulus of elasticity in longitudinal (L), transverse (T) and vertical (V) directions

### 4.6. Sensor Long-Term Performance and Durability

The GFRP material is very durable and has a good long-term stability. However, the property of the host material may change with time, which in turn affects the performance and sensitivity of the GFRP-FBG sensor. To investigate the long-term performance of the developed WIM sensor, this section analyses the impact of the host materials' time-dependent material property on the sensor's durability and long-term stability.

Assuming the host material to be rigid pavement, which is concrete, the Comite´ Euro International du Beton (CEB-FIP) [42] gives a time-dependent MOE as presented below [43]:

$$E_{ci}(t) = \beta_E(t) \times E_{ci} \tag{15}$$

29

where, $E_{ci}(t)$ is the MOE of concrete material at an age of $t$ days, $E_{ci}$ is the MOE of the concrete at an age of 28 days, and is a coefficient depending on the age of concrete (t days) which is given as [43]:

$$\beta_E(t) = (\exp\left[ s(1-(\frac{28}{t})^{0.5}) \right])$$  (16)

where, $t$ is the age of concrete (days), $s$ is a coefficient which depends on the type of cement, $s = 0.20$ for rapid hardening high strength cements, 0.25 for normal and rapid hardening cements and 0.38 for slowly hardening cements.

Figure 17 shows the change of the MOE of concrete using normal and rapid hardening cement which has 2,000 ksi of MOE at 28 days. It can be clearly seen that the MOE of concrete increases significantly with time, especially in the first six years (2,500 days). Figure 18 shows the WIM measurement sensitivity change of the GFRP-FBG sensor in rigid pavement with 2,000ksi MOE with time for 10 years (3,650 days) for its longitudinal, transverse, and vertical components. Table 2 further lists the comparison of sensor sensitivity right after installation and after 10 years for the three sensor components of the GFRP-FBG WIM sensors. After 10 years, the sensitivities of the GFRP-FBG sensor will reduce around 10%. If the original sensitivity is still used after 10 years, the sensitivity reduction of 10% will contribute to the measurement error. Thus, for an accurate WIM measurement using the GFRP-FBG sensors, it is recommended to have a periodical sensor calibration every other year to update the sensor sensitivity function to eliminate the measurement error induced by long-term stability.

Figure 17. The MOE changes of the concrete (2,000 ksi at 28 days) with time (days)
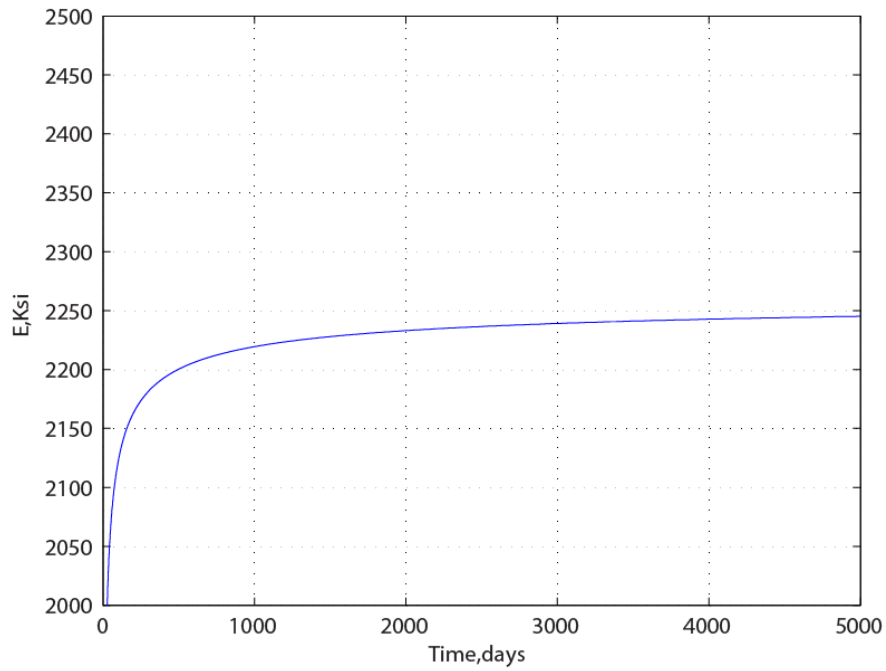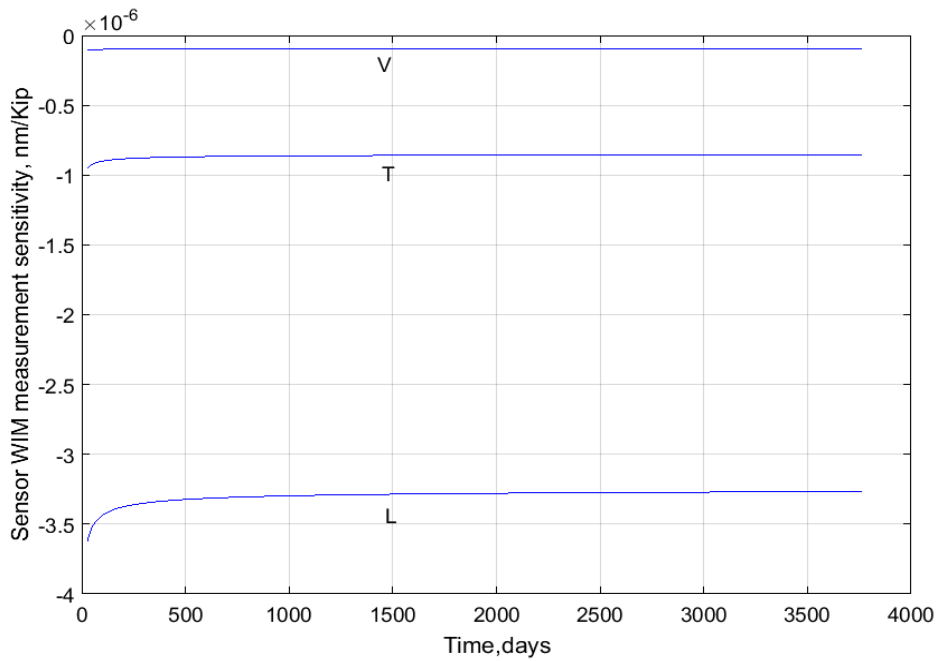


Figure 18. Sensor's WIM measurement sensitivity changes with time in concrete pavement (MOE of 2,000 ksi at 28 days) in longitudinal (L), transverse (T) and vertical (V) directions

Table 2. Comparison of the accuracy of 3D GFRP-FBG sensor after 10 years

| Sensor component | Sensor WIM measurement sensitivity nm/Kip at 28 day | Sensor WIM measurement sensitivity nm/Kip at 3650 days | Absolute Relative error (%) | Accuracy (%) |
|---|---|---|---|---|
| Transverses | $-8.644\times10^{-7}$ | $-7.767\times10^{-7}$ | 10.1 | 89.9 |
| Vertical | $-5.271\times10^{-8}$ | $-4.737\times10^{-8}$ | 10.1 | 89.9 |
| Longitudinal | $-3.625\times10^{-6}$ | $-3.267\times10^{-6}$ | 9.8 | 90.2 |

## 4.7. Summary

In this Chapter, the sensitivity of the GFRP-FBG WIM sensor is evaluated for all significant influencing factors:

1) The GFRP-FBG sensor installation depth influences significantly on the sensor's behaviour for the WIM measurement. The longitudinal component of the GFRP-FBG sensor has the largest WIM measurement sensitivity, which is three times bigger than that in transverse direction. The vertical component yields the smallest WIM measurement sensitivity due to the high stiffness of the pavement panel;

2) Smaller pavement panel will yield a larger WIM measurement sensitivity for the sensor. If the pavement panel has a size larger than 6ft (72 in.), the GFRP-FBG sensor will not be influenced by the changes of panel length anymore;

3) The GFRP-FBG sensor will have maximum sensitivity when the load is in the top of the sensor for all sensor's components. Also, the longitudinal component weight sensitivity may increase by 12.5% if both positive and negative strains are counted for the WIM sensitivity;

4) If a WIM measurement accuracy of 80% is required, the centre of the wheel is required to be passing within 6 inches around the sensor to be effective. For the transverse component, it yields a similar loading range. For the vertical component, the vehicle needs to pass exactly on top of the sensor to achieve an effective measurement;

5) The sensitivity of the sensor is inversely proportional with MOE of the pavement. Therefore, for a more sensitive WIM measurement, a smaller stiffness of the host material is recommended for the GFRP-FBG sensor.

6) The performance of GFRP-FBG sensor for long-term period is performed and come with conclusion that after 10 years, the sensitivities of the 3D GFRP-FBG sensor will reduce around 10%. If the original sensitivity is still used after 10 years. Thus, for an accurate measurement using the developed 3D GFRP-FBG sensors, it is recommended to have a periodical sensor calibration every other year to update the sensor sensitivity function to eliminate the measurement error induced by long-term stability.

## 5. FIELD TESTING OF A CASE STUDY

The developed GFRP-FBG sensor was tested for WIM measurement inside concrete panels at Minnesota's Cold Road Research Facility (MnROAD) of Minnesota Department of Transportation (MnDOT) to validate the theoretical study mentioned in previous chapters.

### 5.1. Background

In order to validate the performance of the GFRP-FBG sensor for WIM measurement, field testing was performed at the Cold Weather Road Research Facility in Minnesota (MnROAD) facility of Minnesota Department of Transportation. MnROAD consists of two unique roadways: a two-lane low-volume loop that is loaded with a 5-axle 80 kips (36,287 kg) semi-truck, and a section of interstate I-94 ''mainline'' that contains two westbound lanes with live traffic. Figure 19(a) shows the two roadway sections. The GFRP-FBG sensor was installed in August 2013 inside one newly casted concrete panel of Cell 40, which belongs to the two-lane low-volume loop as also indicated in Figure 19(a). The GFRP-FBG sensor was installed beneath the wheel path on the concrete panel as shown in Figure 19(b) for the detail layout of the sensor in the panel and in Figure 19(c) for the photo of the sensor installation scene. Table 3 shows the material properties for the GFRP used to package the FBG sensor and the concrete pavement to embed the sensor. Table 4 summarizes the parameters for the installed GFRP-FBG sensor for the field validation tests. All the material property and the installation parameters were provided by MnROAD engineers through filed measurements. These parameters can be input into Equation 12 to obtain the sensor sensitivity for WIM measurements and to measure the WIM in practice.

After the installation of the sensor, the three components of the sensor were connected to a FBG integrator (NI PXIe-4844) together with a temperature compensation FBG sensor. The FBG integrator was further connected to a personal computer to record the data. For WIM measurement

at low speed, it is not required to have a high sampling frequency of the instrument. Therefore, the

sampling rate of the FBG integrator was set to be 10 Hz.  Figures 19(c) and (d) show a photo for

the sensor installation scene for concrete pavement paving.



(a)
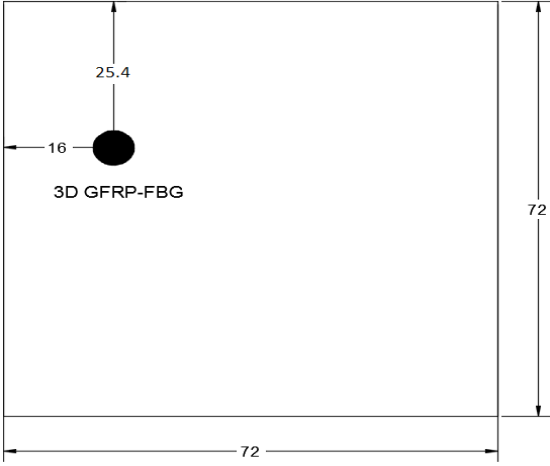


(b)



(c)



(d)

Figure 19. MnROAD facility [44] (a), the layout of the 3D GFRP-FBG sensor inside concrete panel (Unit: inch; 25.4mm) (b), the sensor installation scene (c), and installation scene (d)

Table 3. Material properties [39]

| Material | Modulus of elasticity(E),Klb/in$^2$ | Poisson's ratio |
| --- | --- | --- |
| GFRP | 4,351.14 | 0.3 |
| Concrete | 2,175.57 | 0.2 |

Table 4. Sensor installation parameters for the field validation tests

| Parameter | Longitudinal | Transverse | Vertical |
| --- | --- | --- | --- |
| $x_0$ (in) | 57.1 | 56 | 56 |
| $y_0$ (in) | 25.4 | 26.5 | 25.4 |
| $\varphi$ | 0.975 | 0.975 | - |
| E(psi) | | 2,175,566 | |
| $\eta$ (in) | 25.4 | 26.5 | 25.4 |
| h(in) | | 3 | |
| $h_0$(in) | 2 | 2 | 0.95 |
| a(in) | | 72 | |
| b(in) | | 72 | |
| k(pci) | | 1078 | |

## 5.2. Field Testing Results

To perform the validation tests, a -5-axle semi-truck with total gross weight of 80 Kips (36.29 tons) was used to generate the weight to be measured in motion. The truck moves on top of the sensor back and forth at 5 mph. Figure 20(a) shows of the axle load distribution of the truck at each axle and Figure 20(b) shows the test scene.



| | |
| --- | --- |
| (a) | (b) |
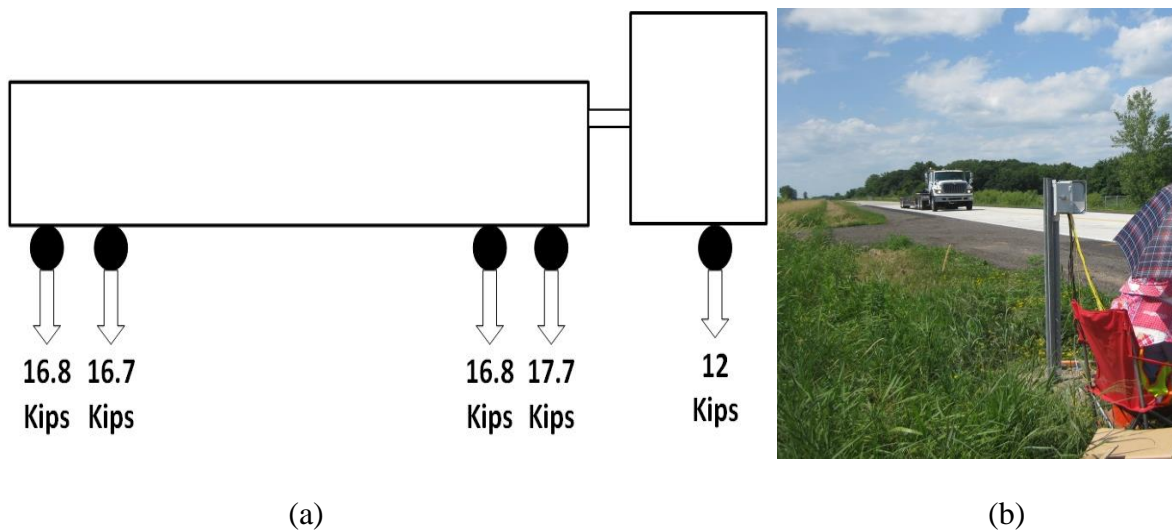
Figure 20. Layout of MnROAD loading truck (a) and field test scene (b)

Figures 21(a~c) shows the sensor's responses on its longitudinal, transverse, and vertical components for one truck passed on the concrete panel at MnROAD facility at September 2014. All the three components of the GFRP-FBG sensor clearly identify each axle of the truck. The sensor responses illustrated that the longitudinal component of the sensor has the largest sensitivity for the WIM and showed the most promising performance.
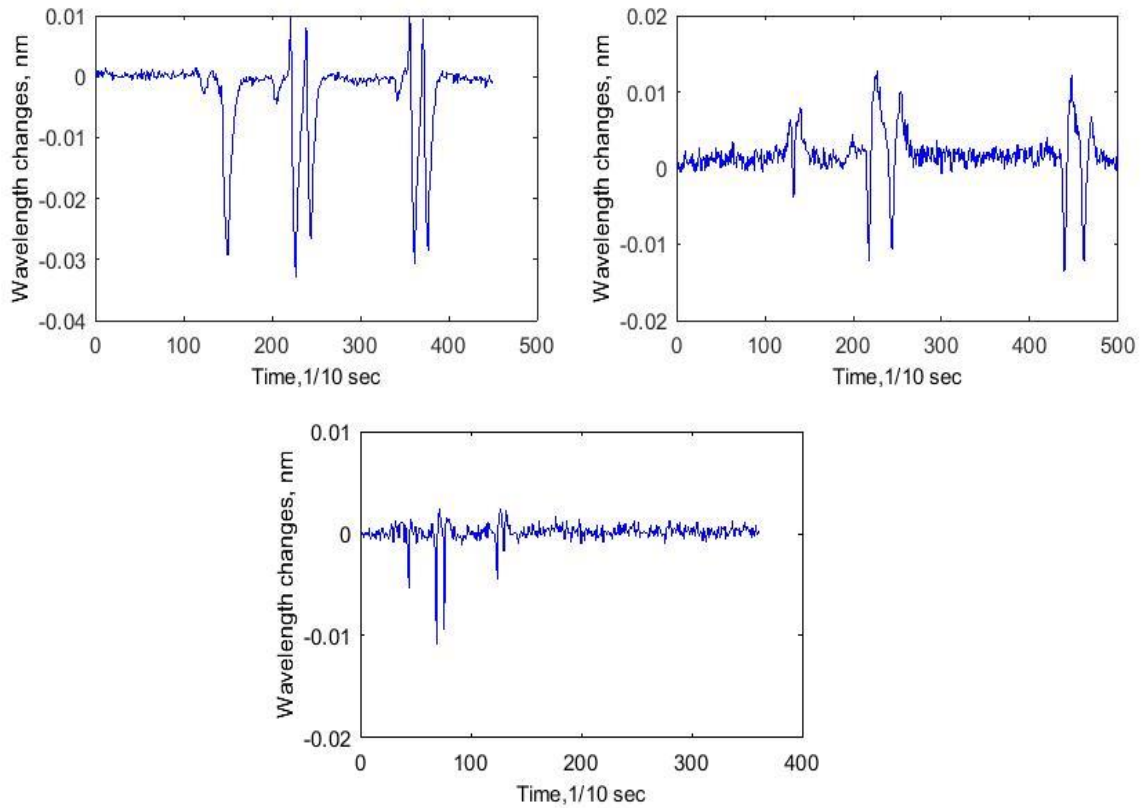


Figure 21. The responses from 3D GFRP-FBG sensor in longitudinal (a), transverse (b), and vertical directions (c)

Based on the Equation 12 and the parameters provided in Table 4, the theoretic WIM measurement sensitivity of the GFRP-FBG sensor in case study can be calculated as $-2.395 \times 10^{-3}$ pm/Kip, $-0.807 \times 10^{-3}$ pm/Kip and $-0.701 \times 10^{-3}$ pm/Kip for longitudinal, transverse, and vertical components, respectively. According to the calculated sensitivity and the measured wavelengths

in Figure 21, Table 5 summarize the WIM measurements from the longitudinal, transverse, and vertical components of the GFRP-FBG sensor for each truck axle, respectively.

Table 5. Field WIM measurements from the sensor

| Sensor Component | | Axle 1 | Axle 2 | Axle 3 | Axle 4 | Axle 5 |
|---|---|---|---|---|---|---|
| Longitudinal | Wavelength changes (pm) | -29.4 | -32.8 | -26.7 | -30.8 | -28.4 |
| | WIM (kips) | 8.0 | 8.95 | 7.7 | 8.4 | 7.8 |
| Transverse | Wavelength changes (pm) | -3.7 | -12.1 | -10.6 | -13.4 | -12.2 |
| | WIM (kips) | 3.0 | 9.77 | 8.6 | 10.8 | 9.85 |
| Vertical | Wavelength changes (pm) | -5.3 | -10.8 | -9.3 | -4.4 | -1.7 |
| | WIM (kips) | 5.0 | 10.1 | 8.7 | 4.1 | 1.6 |

## 5.3. Repeatability

To test the repeatability of the sensor, the truck was driving back and forth for three times across the sensor location. Since the longitudinal component of the sensor has the best performance, in this study, only the repeatability of the longitudinal component of the sensor was tested. Figure 22 and Table 6 show the WIM responses of the longitudinal component of the sensor under repeated truck loading. The longitudinal component of the sensor has a very good repeatability of 90%.
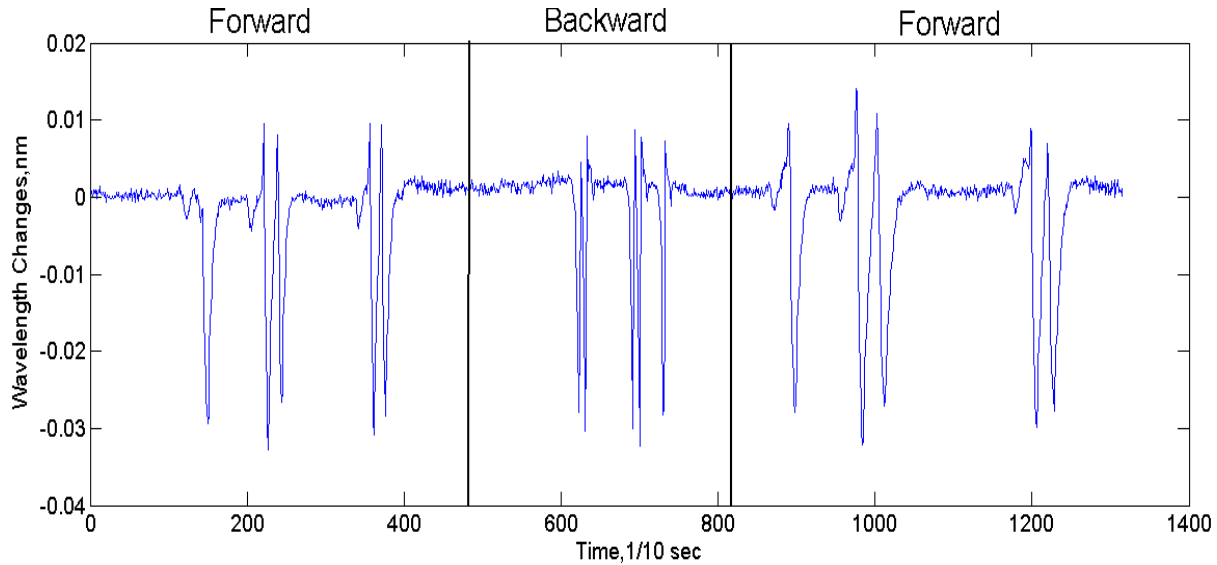
Figure 22. Repeatability test results of the longitudinal component of the sensor

Table 6. Repeatability test results of the longitudinal component of the sensor

| Longitudinal sensor | | Axle 1 | Axle 2 | Axle 3 | Axle 4 | Axle 5 |
|---|---|---|---|---|---|---|
| First run | wavelength changes (pm) | -29.4 | -32.8 | -26.7 | -20.8 | -28.4 |
| | WIM (kips) | 8 | 8.95 | 7.7 | 8.4 | 7.8 |
| Second run | wavelength changes (pm) | -27.4 | -32.3 | -30.0 | -30.30 | -27.9 |
| | WIM (kips) | 7.48 | 8.82 | 8.19 | 8.27 | 7.61 |
| Third run | wavelength changes (pm) | -27.9 | -32.15 | -27.18 | -29.9 | -27.8 |
| | WIM (kips) | 7.61 | 8.8 | 7.42 | 8.16 | 7.59 |

## 5.4. Dynamic Range

The dynamic range for the GFRP-FBG sensor was calculated from Equation 13 and summarized in Table 7. The dynamic range calculated for the maximum strains of the host material (concrete in this case) to handle. For concrete, the typical maximum strain is equal to 1,000 $\mu\varepsilon$. It is clear that the dynamic range in terms of changing in wavelength for all the sensor is approximately close to each other but in terms of weights the longitudinal component has the minimum dynamic range of 331 Kips because it has high sensitivity following by transverse and vertical.

39

Table 7. Dynamic range for 3D GFRP-FBG sensor

| Sensor | $\lambda$ (nm) | $\Delta\lambda$ (nm) | $P_{max}$ (Kips) |
|--------|---------------|---------------------|------------------|
| L | 1529.137653 | 1.212 | 331 |
| T | 1534.517604 | 1.216 | 982 |
| V | 1524.920018 | 1.209 | 1131 |

## 5.5. Comparison Between Theoretical Analysis and Field Testing Result

Table 8 compares the WIM measurements from the longitudinal, transverse, and vertical components of the GFRP-FBG sensor with the reference weights for each truck axle respectively. When compared with the reference weight which are the actual weights om the truck tires, the longitudinal, transverse, and vertical components of the sensor have measurement accuracy of 90%, 79%, and 67%, respectively. The comparison shows that the longitudinal component of the GFRP-FBG sensor has the best WIM measurement performance, followed by the transverse component. The vertical component of the sensor, since it requires the truck to drive exactly on top of the senor head, which is very hard to control in practice, has the lowest measurement accuracy in field testing. Thus, for practical applications, the longitudinal GFRP-FBG sensor is recommended for WIM measurement at low speed.

Table 8. Comparison of the WIM measurements with references

| Measured Weight | Axle 1 | | Axle 2 | | Axle 3 | | Axle 4 | | Axle 5 | |
|-----------------|--------|--------|--------|--------|--------|--------|--------|--------|--------|--------|
| | WIM (Kips) | Error (%) | WIM (Kips) | Error (%) | WIM (Kips) | Error (%) | WIM (Kips) | Error (%) | WIM (Kips) | Error (%) |
| Reference | 5.8 | - | 9.05 | - | 8.05 | - | 8.6 | - | 8.2 | - |
| Longitudinal Component | 8 | 38 | 8.95 | 1.1 | 7.7 | 4.3 | 8.4 | 2.3 | 7.8 | 4.9 |
| Transverse Component | 3.1 | 46.5 | 9.77 | 8 | 8.6 | 7 | 10.8 | 25.6 | 9.85 | 20.1 |
| Vertical Component | 5 | 13.7 | 10.1 | 11.6 | 8.7 | 8.1 | 4.1 | 52.3 | 1.6 | 80.5 |

## 5.6. Summary

In this Chapter, the field test results which collected from case study of concrete panels at MnROAD validate the theoretical study:

1) The theoretical weight sensitivity is $-2.395 \times 10^{-3}$ pm/Kip, $-0.807 \times 10^{-3}$ pm/Kip and $-0.701 \times 10^{-3}$ pm/Kip for longitudinal, transverse, and vertical components, respectively;

2) The longitudinal component of the GFRP-FBG sensor has the best WIM measurement performance, followed by the transverse component and vertical component;

3) The longitudinal component result with minimum average relative error among the other component with 10%, both transverse and vertical components shows high relative error with 21% and 33% respectively;

4) The longitudinal component seems to be the most accurate sensor of 90% and has a very good repeatability of 90%;

5) The longitudinal component has the minimum dynamic range of 331 Kips because it has high sensitivity following by transverse and vertical components.

# 6. CONCLUSIONS AND FUTURE WORK

This thesis introduced a GFRP-FBG sensor which can be installed inside pavements for WIM measurements at vehicle driving speed up to 25 mph. Theoretical derivation and sensitivity study were performed followed by field experiments in a specific case study to validate the theoretical study. The conclusions of this thesis can be drawn as follows:

1) A general WIM measurement sensitivity function can be derived for the GFRP-FBG sensor, which can use to guide the measurements;

2) The GFRP-FBG sensor is very sensitive to the sensor installation depth and the best performance is to install the sensor at the bottom of the pavement sections. If the sensor is installed in the middle of the pavement panel, the sensor will not be effective for WIM measurements;

3) If the length of the pavement panel is larger than 6ft (72 in), the sensor sensitivity will not affect much for increasing the pavement panel size;

4) The transverse loading location of the vehicle wheel is a critical factor for using the GFRP-FBG sensor for WIM measurements. To obtain a measurement accuracy of 80% or above, the center of the wheel is required to be passing within 6 inches around the sensor. With sufficient distance between wheels, the influence from the neighbour wheel can be neglected and two sensors will be required to measure axle weight if needed;

5) The GFRP-FBG sensor is expected to have a good long-term durability. For a service life of 10 years, it will introduce a long-term stability error within 10%;

6) Field testing validated that the GFRP-FBG sensor has a measurement accuracy of 90%, 79%, and 67% for longitudinal, transverse, and vertical components. Thus, it is obvious

that the best orientation of the GFRP-FBG WIM sensor is along the wheel path to get

maximum sensitivity with accuracy above 90%.

This study can serve as a reference to guide the use of the developed GFRP-FBG sensors

for WIM measurements at low speed up to 25mph without consideration of dynamic effects. Future

efforts will apply to evaluate the performance of the GFRP-FBG sensor for high-speed beyond

25mph of vehicle driving speed to consider how the dynamic effect will affect the measurements.

Also, evaluate the performance of the GFRP-FBG sensor in different host material such as a

flexible pavement. The numerical study will be provided in future to verify the performance of

this sensor in rigid pavement.

# REFERENCES

[1]     Sullivan DE. Materials in use in US interstate highways. Geological Survey fact sheet 2006-3127. Washington, DC: USG. 2006.

[2]     Highway Pavement; [accessed 20 Mar 2016]. Available from: http://www.cement.org/think-harder-concrete/paving/concrete-pavement/highways.

[3]     Delatte NJ. Concrete pavement design, construction, and performance. CRC Press; 2014 May 22.

[4]     Mathew TV, Rao KK. Introduction to Transportation engineering. Civil Engineering–Transportation Engineering. IIT Bombay, NPTEL ONLINE, http://www. cdeep. iitb. ac. in/nptel/Civil% 20Engineering. 2006 Oct 19.

[5]     Russel W, Lenz, P.E., Director, Construction Division. Pavement Design Guide Manual. Texas Department of Transportation. Texas: Texas Department of Transportation. Retrieved from http://onlinemanuals.txdot.gov/txdotmanuals/pdm/index.htm. 2011.

[6]     Florida Department Of Transportation (FDOT), pavement management office. Rigid pavement design manual. Document No. 625-010-006-e.Florida. January 2009.

[7]     Kher RK, Hudson WR, McCullough BF. A Systems Analysis of Rigid Pavement Design. No.123-5. 1971 Jan.

[8]     Module II: Analysis and design of concrete pavements: Lecture 2: Analysis of Concrete Pavement;[accessed 5May 2016]. Available from: http://nptel.ac.in/courses/Webcourse-contents/IIT-KANPUR/transport_e/TransportationII/ui/framset-m2-l2.htm.

[9]     Kumara MA. Analysis and Verification of Stresses and Strains and Their Relationship to Failure in Concrete Pavements under Heavy Vehicle Simulator Loading [Doctoral dissertation].Florida: University of Florida; 2005.

[10]    Hall KT. State of the art and practice in rigid pavement design. Transportation in the New Millennium. 2000.

[11]    Tom VM, Krishna Rao KV. Introduction to transportation engineering. Marshall Mix Design, National Programme on Technology Enhanced Learning (NPTEL), Indian Institute of Technology, India. 2007.

[12]    Fernando EG, Middleton D, Carlson TB, Longmire R, Sepulveda ED, Ruback LG, Freeman TJ, Oh J. Deploying Weigh-in-motion Installations on Asphalt Concrete Pavements. No. FHWA/TX-09/0-5551-1. 2009 Feb.

[13]    Jacob B, Feypell-de La Beaumelle V. Improving truck safety: Potential of weigh-in-motion technology. IATSS research. 2010 Jul 31, 34(1):9-15.

[14]    Taylor B, Bergan A, Lindgren N, Eng CB. The importance of commercial vehicle weight enformcement in safety and road asset management. Annual Review pp. 2000 Jan, 234:237.

[15]    Jinwoo Brian LE, Hanseon CH. Commercial Vehicle Preclearance Program: Motor Carriers' Perceived Impacts and Attitudes towards Potential Implementation. In Proceedings of the Eastern Asia Society for Transportation Studies 2013 (Vol. 9).

[16]    Szary PJ, Maher A. Implementation of Weigh-in-motion (WIM) Systems. No. FHWA-NJ-2009-001. 2009 Feb.

[17]    Robert FL, Kandhal PS, Brown ER, Lee DY, Kennedy TW, Hot Mix Asphalt Materials, Mixture Design, and Construction, NAPA Education Foundation, Second Edition, Lanham, Maryland, 1996.

[18]    Peters B, Koniditsiotis C. Weigh-In-Motion Technology. (ISBN085588553X) Austroads project No. RUM. TM. 2000, 9.

[19]     Liu R, Chen X, Li J, Guo L, Yu J. Evaluating innovative sensors and techniques for measuring traffic loads: final report. Technical Report, Houston, USA, 2006.

[20]     U.S. Department of Transportation, Federal Highway Administration, Office of Freight Management Operations, Freight Analysis, version 3, 2010.

[21]     Wierzba P, Kosmowski BB. Polarimetric sensor for weigh-in motion of road vehicles. Opto-Electronics Review. 2000, 8:181-7.

[22]      ASTM Standard E1318-02, Highway Weigh-in-Motion (WIM) Systems with User Requirements and Test Methods, Annual Book of ASTM Standards, 2002.

[23]     Bushman R, Pratt AJ. Weigh in motion technology–economics and performance. InPresentation on the North American Travel Monitoring Exhibition and Conference (NATMEC). Charlotte, North Carolina 1998 May.

[24]     Martin PT, Feng Y, Wang X. Detector technology evaluation. Mountain-Plains Consortium; 2003 Nov.

[25]     Lee B. Review of the present status of optical fiber sensors. Optical fiber technology. 2003 Apr 30, 9(2):57-79.

[26]     Majumder M, Gangopadhyay TK, Chakraborty AK, Dasgupta K, Bhattacharya DK. Fibre Bragg gratings in structural health monitoring—present status and applications. Sensors and Actuators A: Physical. 2008 Sep 15, 147(1):150-64.

[27]     Zhang L, Haas C, Tighe SL. Evaluating Weigh-In-Motion Sensing Technology for Traffic Data Collection. InAnnual Conference of the Transportation Association of Canada 2007 (pp. 1-17).

[28]     Malla RB, Sen A, Garrick NW. A special fiber optic sensor for measuring wheel loads of vehicles on highways. Sensors. 2008 Apr 11, 8(4):2551-68.

[29] Sidek O, Kabir S, Afzal MH. Fiber Optic-based Sensing Approach for Corrosion Detection. InProgress in Electromagnetics Research Symposium (PIERS) Proceedings, Suzhou, China 2011 Sep (pp. 642-6).

[30] Hill KO, Meltz G. Fiber Bragg grating technology fundamentals and overview. Journal of lightwave technology. 1997 Aug 8, 15(8):1263-76.

[31] Meller SA, de Vries MJ, Arya V, Claus RO, Zabaronick N. Advances in optical fiber sensors for vehicle detection. InIntelligent Systems & Advanced Manufacturing 1998 Jan 27 (pp. 318-322). International Society for Optics and Photonics.

[32] Wang K, Wei Z, Chen B, Cui HL. A fiber-optic weigh-in-motion sensor using fiber Bragg gratings. InOptics East 2005, 2005 Nov 9 (pp. 60040S-60040S). International Society for Optics and Photonics.

[33] Moyo P, Brownjohn JM, Suresh R, Tjin SC. Development of fiber Bragg grating sensors for monitoring civil infrastructure. Engineering structures. 2005 Oct 31, 27(12):1828-34.

[34] Berardis S, Caponero MA, Felli F, Rocco F. Use of FBG sensors for weigh in motion. InBruges, Belgium-Deadline Past 2005 May 23 (pp. 695-698). International Society for Optics and Photonics.

[35] Casas JR, Cruz PJ. Fiber optic sensors for bridge monitoring. Journal of Bridge Engineering. 2003 Nov, 8(6):362-73.

[36] Udd E, Kunzler M, Laylor HM, Schulz WL, Kreger ST, Corones JC, McMahon R, Soltesz SM, Edgar R. Fiber grating systems for traffic monitoring. In6th Annual International Symposium on NDE for Health Monitoring and Diagnostics 2001 Aug 3 (pp. 510-516). International Society for Optics and Photonics.

[37]     Oh HS, Sim J. Interface debonding failure in beams strengthened with externally bonded GFRP. Composite Interfaces. 2004 Jan 1, 11(1):25-42.

[38]     Zhou Z, Liu W, Huang Y, Wang H, Jianping H, Huang M, Jinping O. Optical fiber Bragg grating sensor assembly for 3D strain monitoring and its case study in highway pavement. Mechanical Systems and Signal Processing. 2012 Apr 30, 28:36-49.

[39]     Zhang Z, Huang Y, Palek L, Strommen R. Glass fiber–reinforced polymer–packaged fiber Bragg grating sensors for ultra-thin unbonded concrete overlay monitoring. Structural Health Monitoring. 2015, 14(1):110-23.

[40]     Fundamentals of FBG Optical Sensing; June 28, 2011 [accessed 10 Dec 2015]. Available from: http://www.ni.com/white-paper/11821/en/.

[41]     Zhang Z, Huang Y, Bridgelall R, Palek L, Strommen R. Sampling optimization for high-speed weigh-in-motion measurements using in-pavement strain-based sensors. Measurement Science and Technology. 2015 May 6, 26(6):065003.

[42]     Comite´ EuroInternational du Be ´ton (CEB-FIP), CEB-FIP Model Code (2010).

[43]     Singh BP, Yazdani N, Ramirez G. Effect of a time dependent concrete modulus of elasticity on prestress losses in bridge girders. International Journal of Concrete Structures and Materials. 2013 Sep 1, 7(3):183-91.

[44]     Burnham T. Thin concrete pavements and overlays—ongoing MnROAD research. InMnDOT, Presented in 2013 NCC Spring Meeting, Philadelphia, PA 2013 Apr.